Structural, Electronic and Magnetic Properties of the Heusler Alloy Mn_2VIn: A Combined DFT and Experimental Study

Zipporah W. Muthui[1,2,3], Robinson J. Musembi[1], Julius M. Mwabora[1], Ralph Skomski[4], and Arti Kashyap[2]

[1]Department of Physics, University of Nairobi, Nairobi 30197-00100, Kenya
[2]School of Basic Sciences, Indian Institute of Technology, Mandi, Himachal Pradesh 175005, India
[3]Chuka University, Chuka 109-60400, Kenya
[4]Nebraska Center for Materials and Nanoscience, Department of Physics and Astronomy, University of Nebraska, Lincoln, NE 68588 USA

Structural, electronic and magnetic properties of the Heusler alloy Mn_2VIn have been investigated using the density functional theory and experimental techniques. Unlike many other Heusler compounds, Mn_2VIn is not predicted to be half-metallic at the optimized lattice constant, but is highly spin polarized at a slightly lower lattice constant. It however exhibits ferrimagnetic coupling between the Mn and V sublattices, as expected of Mn-based Heuslers. We have, then, synthesized the compound by arc melting and studied magnetic properties that are of interest fundamentally and for technological applications. The structural properties were determined using X-ray diffraction, revealing the presence of cubic and tetragonal phases in the sample. The chemical composition was determined using energy-dispersive X-ray spectroscopy together with the scanning electron microscope, and the magnetic properties were investigated by superconducting quantum interference device magnetometry. The alloy exhibits superparamagnetic spin blocking with a blocking temperature T_B of 40 K.

***Index Terms*—Density functional theory (DFT), electronic structure, Heusler compounds, superparamagnetism.**

I. Introduction

HEUSLER alloys of composition X_2YZ, where X and Y are transition metal elements and Z is a main group element, exhibit technologically useful properties such as high spin polarization at the Fermi level and high Curie temperatures. These properties are particularly relevant in the development of spintronic devices such as magnetic tunneling junctions [1]. While half-metallic ferromagnetism frequently occurs in Heusler compounds in which $X = \text{Co}$, ferrimagnetism is common in Heusler compounds having $X = \text{Mn}$, such as Mn_2VAl and Mn_2CoGa [2]. Heusler compounds are very versatile and have been shown to display a wide range of other intriguing properties such as martensitic transformations and superparamagnetism.

Martensitic transformations have the potential to exhibit the magnetic shape memory effect, which can be exploited in sensors and actuators. A well-known example is Ni_2MnGa [3]. The structural transitions are often accompanied by magnetic transitions that go beyond Curie and Néel transitions, and some Heusler alloys exhibit superparamagnetism and spin-glass effects [4], [5]. Furthermore, tetragonal distortions involved in martensitic transitions yield magnetocrystalline anisotropy, which is useful for some applications.

Multiple magnetic transitions, similar to those in ternary intermetallic compounds such as Ho_2Ni_2Pb [6], have also been observed in some Heusler alloys. In arc-melted samples of the semi Heusler $Cu_{1-x}Ni_xMnSb$, a bifurcation of the field-cooled (FC) and zero-FC (ZFC) curves and a constant value of magnetization in the FC curve points to the presence of competing antiferromagnetic (AFM) and ferromagnetic (FM) interactions [7].

Superparamagnetism, which is often observed in nanoparticle systems, is rare in Heusler compounds. Fe_2VAl, Fe_2VGa, Fe_2TiSn, Ni_2MnIn, Ni_2FeAl, $Ni_{50}Mn_{25+y}X_{25-y}$, $Fe_{2+x}V_{1-x}Al$, and $Fe_{2+x}V_{1-x}Ga$ are among the systems where superparamagnetism has been observed [5], [8]–[10]. These superparamagnetic alloys are being investigated in the context of nanogranular giant magnetoresistive (GMR) sensors [11]. Other potential applications include magnetic resonance imaging contrast agents, ferrofluid technology, and heat transfer.

Superparamagnetic materials, spin glasses, and cluster-glass materials, also some bulk magnets display similar features on their FC/ZFC curves below the blocking temperature (T_B), which results in irreversibility [12]. A peak in the FC curve can have various reasons, including domain-wall pinning. Superparamagnetism occurs above the blocking temperature and is typically characterized by a very small hysteresis. One example is $Cu_2Mn_{0.75}Fe_{0.25}Al$ alloy, where the coercive field H_C is 30 Oe above 60 K and negligible above 200 K [12].

The focus of this paper is on vanadium-containing Heuslers. Some of these alloys exhibit segregation problems. For example, Lue *et al.* [13] attempted to use arc-melting to prepare half-Heusler CoVSn but clearly identified $CoSn_2$, CoSn, and V_2Sn_3 phases. Magnetic defects caused by Fe antisite disorder in $Fe_{2+x}V_{1-x}Al$ and $Fe_{2+x}V_{1-x}Ga$, was found to be responsible for the previously reported GMR behavior, with Fe_2VGa having the highest GMR effect of approximately 50%

Manuscript received July 4, 2017; revised August 7, 2017 and September 6, 2017; accepted September 20, 2017. Date of publication December 4, 2017; date of current version December 20, 2017. Corresponding author: A. Kashyap (e-mail: arti@iitmandi.ac.in).

Color versions of one or more of the figures in this paper are available online at http://ieeexplore.ieee.org.

Digital Object Identifier 10.1109/TMAG.2017.2756618

reported for magnetically dilute or granular 3*d* transition metal alloys [14].

To the best of our knowledge, the properties of the Heusler compound Mn_2VIn have not been investigated so far. In this paper, we use the density functional theory (DFT) to determine the ground state structural, electronic and magnetic properties of Mn_2VIn and experimentally investigate the system by arc melting under an argon atmosphere, using high-purity Mn, V and In. We have, then, performed structural characterization using X-ray diffraction (XRD) and determined the magnetic properties using a superconducting quantum interference device (SQUID). We determined the composition and homogeneity of the arc-melted sample using a scanning electron microscope together with energy-dispersive X-ray spectroscopy (EDXS-SEM).

II. Theoretical and Experimental Methods

A. Computational Details

The spin-polarized DFT calculations used to determine the structural, electronic and magnetic properties of Mn_2VIn were implemented in the Vienna Ab Initio Simulation Package. We used the self-consistent projector augmented wave approach, employing the Perdew-Burke-Ernzerhof parameterization of the generalized gradient approximation, to treat the exchange and correlation in the system. The unit cell was modeled as a stoichiometric $L2_1$ full Heusler structure, space group (SG) 225, with Wyckoff positions of 8c (1/4, 1/4, 1/4), 4b (1/2, 1/2, 1/2), and 4a (0, 0, 0) for Mn, V and In, respectively. A Monkhorst–Pack uniform K point grid with $21 \times 21 \times 21$ k points was chosen for geometry optimization and static total energy calculations. The geometries were optimized by relaxing both the unit cell and the positions of all the atoms within the unit cell using the conjugate-gradient algorithm, until a stopping criterion of energy change less than 10^{-6} eV was reached. The integration over the irreducible part of the Brillouin zone was done using the linear tetrahedron method with Blöchl corrections, using uniform cut-off energy of 430 eV, with the energy convergence criterion set at 10^{-7} eV.

B. Experimental Details

Approximately 2 g of Mn_2VIn ingots were prepared by arc melting of stoichiometric amounts of the constituent high purity elements using the Edmund Buhler GmbH MAM 1 arc-melting furnace. The melting was carried out in a high-purity argon atmosphere to avoid oxygen contamination. Before the melting, a Ti ball was used to bind the remaining oxygen. To ensure homogeneity, the sample was re-melted several times and subsequently annealed at 450 °C for 21 days before being slowly cooled to room temperature. The composition and homogeneity were determined by EDXS-SEM. The structure was determined using XRD, and Rietveld refinement was done using FULLPROF software. The magnetization measurements were performed on SQUID magnetometer.

III. Results and Discussion

In this section, we present the results of our theoretical calculations and measurements.

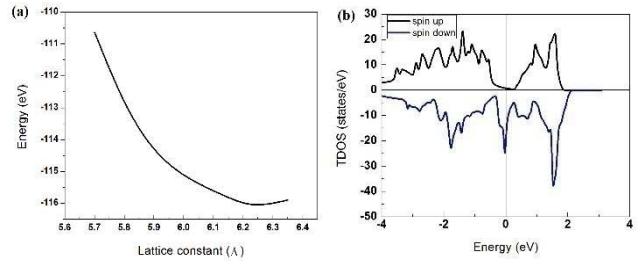

Fig. 1. Theoretical lattice constants and densities of states for $L2_1$-ordered Mn_2Vin. (a) Volume optimization for Mn_2Vin. (b) TDOS for Mn_2VIn for a compressed lattice having $a = 5.83$ Å. The spin polarization in (b) is 94.7%.

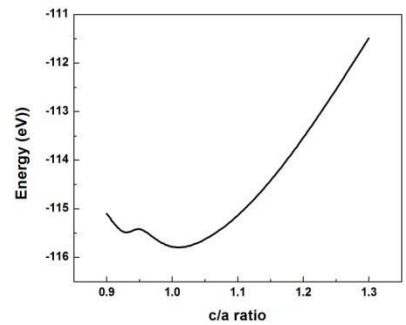

Fig. 2. Dependence of the calculated total energy on lattice-constant ratio *c*/*a*.

A. Theoretical Results

The optimized lattice constant for cubic $L2_1$-ordered Mn_2VIn is $a = 6.25$ Å, as shown in Fig. 1(a). The analysis of the corresponding atomic spin directions reveals a ferrimagnetic spin structure where the Mn, V and In moments are 3.01, -1.99, and -0.05 μ_B, respectively, and the net magnetization is 3.98 μ_B per formula unit (f.u.). The density of states show that the alloy is not half-metallic, and the same conclusion can be drawn from the Slater-Pauling rule for half-metallic Heusler compounds, which predicts a magnetic moment of 2 μ_B per formula unit. This is due to the large atomic radius of In, 1.63 Å, compared to 1.37 Å for Mn and 1.31 Å for V. This causes the lattice parameter of the optimized structure to be rather large, suppressing the *d*-*d* hybridization responsible for the formation of the half-metallic gap.

To further elucidate this point, we used DFT calculations to perform a gedanken experiment where the lattice is compressed until $a = 5.83$ Å, substantially enhancing the *d*-*d* hybridization. This lattice parameter corresponds to the $L2_1$ phase in our arc-melted sample (Section III-B). The spin structure remains ferrimagnetic, but the respective atomic moments of Mn, V and In change to 1.38 μ_B, -0.88 μ_B, and -0.01 μ_B. The net magnetization of 1.87 μ_B is close to the Slater-Pauling prediction of 2 μ_B, and the total density of states (TDOS), Fig. 1(b), shows that the compressed alloy is essentially half-metallic, with a spin polarization of 94.6% at the Fermi level.

Some Heuslers, such as Ni_2MnGa, exhibit a tetragonal distortion [15]. To estimate the effect of a tetragonal distortion on the total energy of Mn_2VIn, we have performed DFT calculations for different *c*/*a* ratios from 0.9 to 1.1. For simplicity, we have used $a = 6.25$ Å for all aspect ratios. Fig. 2 shows

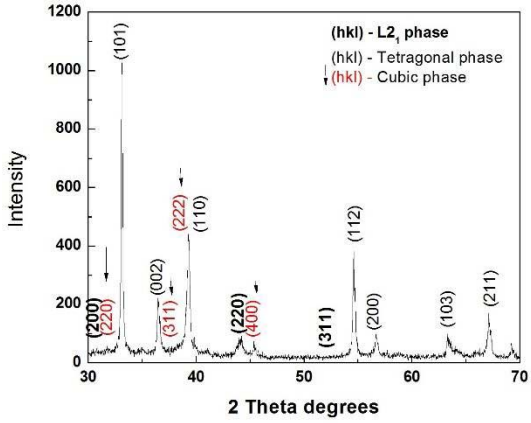

Fig. 3. XRD pattern for Mn_2VIn arc-melted sample. The $L2_1$ structure peaks are labeled in bold while the tetragonal peaks are labeled normally. The arrows indicate the third cubic phase (SG 227).

the total energy as a function of the c/a ratio, which was varied independently of a. The curve shows a shallow local minimum at $c/a = 0.93$, lying 412 meV above the global minimum. The shallow minimum may indicate the vicinity of a martensitic phase transition, associated with the shape memory effect. The total magnetic moment of the tetragonally distorted Mn_2VIn with a c/a ratio of 0.93 is 2.557 μ_B per formula unit. The Mn and V atoms have antiparallel moments of 1.949 μ_B and -1.296 μ_B, respectively, whereas the In moment is negligible at -0.045 μ_B. The resulting electronic structure has a spin polarization of 51.6% at the Fermi level.

B. Experimental Results

Fig. 3 shows the XRD pattern of the arc-melted sample, obtained from Cu $K\alpha$ powder XRD. Three phases have been identified through Rietveld refinement: 8.00% cubic $L2_1$, SG 225, 35.12% of an unknown tetragonal phase having SG 139, and 56.88% of a cubic phase having the SG 227. The observed phase with SG 227 may be the B32a phase (prototype NaTl), one of the ordering variants of Heusler compounds in which the X atoms of one sublattice intermix with the Y sites, while the other X atoms mix with the Z sites [16]. The experimental lattice parameters are $a = 5.83$ Å ($L2_1$ phase), $a = b = 3.26$ Å and $c = 4.95$ Å (tetragonal phase), and $a = 7.95$ Å (second cubic phase).

In Fig. 3, the peaks indexed to the cubic $L2_1$ phase include the (220), (311), and (200) reflections, labeled by bold indices. The (200) peak is very weak and the (311) peak is virtually invisible. Weak or invisible (200) and (311) peaks are frequently encountered in Heusler alloys and reflect chemical disorder, small atomic contrast between iron-series elements, and, in the present system, the low fraction of the $L2_1$ phase. The peaks indexed to the tetragonal phase are (101), (002), (110), (112), (200), (103), and (211), while the arrows point to (220), (311), (222), and (400) reflections of SG 227 cubic phase.

Fig. 4 shows the EDX spectrum for a region in the SEM image (inset). The composition derived from the EDX spectrum is $Mn_{2.29}V_{0.6}In$, or, using atomic percentages, $Mn_{59}V_{15}In_{26}$. This composition indicates that one or more of the phases in the ingot are off-stoichiometric compared to the ideal Mn_2VIn composition. While adding further complexity to the system, this off-stoichiometry explains why the experimental lattice constants differ from the theoretical predictions.

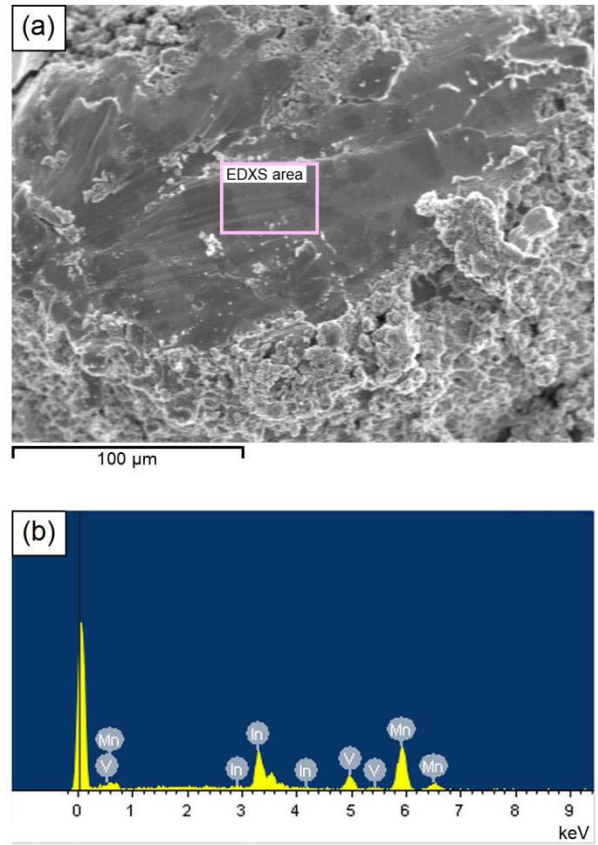

Fig. 4. (a) SEM micrograph with the small area in the inset corresponding to the $Mn_{2.29}V_{0.6}In$ composition. (b) Corresponding EDXS analysis spectrum.

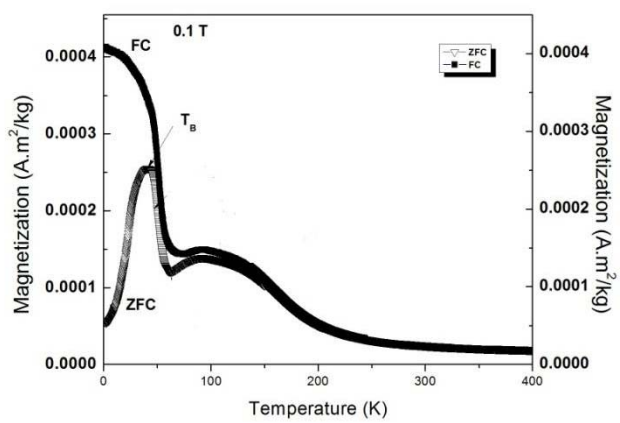

Fig. 5. ZFC and FC curves for the Mn-V-In ingot.

Two types of magnetic measurements have been performed, namely, FC/ZFC experiments in a magnetic field of 0.1 T and hysteresis loops in fields of up to 7 T. Fig. 5 shows the ZFC and FC magnetization curves. The appearance of two maxima indicates that the sample contains two magnetic

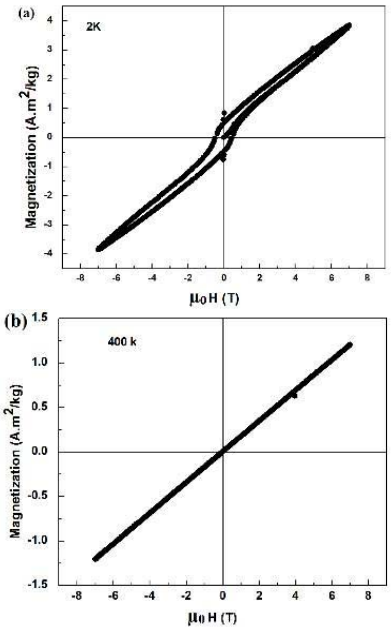

Fig. 6. Hysteresis loops of the Mn-V-In sample: (a) at 2 K and (b) at 400 K.

phases or regions [17]. The regions or phases may be associated with the phases identified by XRD or correspond to X-ray amorphous grain-boundary regions. The Curie-like temperature dependence of the magnetization and its small magnitude (about 0.001 μ_B/f.u.) speak in favor of small superparamagnetic inclusions or clusters in a nonmagnetic matrix, as contrasted to ferro- or ferrimagnetic phases with long-range magnetic order and well-defined Curie temperatures. Judging from the Curie-like tail of the FC/ZFC curves, the size of the clusters is about 800 μ_B, roughly corresponding to an average cluster size of about 3 nm.

In Fig. 5, there are two bifurcations, one for each magnetic subsystem. The one occurring at lower temperatures is labeled as T_B (blocking temperature) for convenience. Such blocking effects are frequently encountered in nanostructures [18] and other systems [19]–[24] and primarily caused by magnetocrystalline anisotropy. Below the blocking temperature, thermal excitations are no longer able to overcome the micromagnetic energy barriers caused by the magnetocrystalline anisotropy, so the ZFC and FC curves behave differently. There are many types of energy barriers, which make it difficult to physically interpret blocking temperatures.

Fig. 6 shows the hysteresis loops at low temperature (2 K) and above room temperature (400 K).

The low temperature measurement (a) yields substantial hysteresis, with a coercivity of about 0.5 T, whereas the hysteresis and coercivity are negligible above room temperature (b). This is consistent with Fig. 5: hysteresis and coercivity correspond to bifurcation, which is fully developed below $T_B \approx 40$ K, whereas 400 K is well above the onset of bifurcation. An interesting feature of Fig. 6 is the pronounced high-field slope, whose visibility is enhanced by the smallness of the magnetic signal. This slope is probably caused by the Pauli paramagnetism of one or more of the three main phases. Another possible explanation is an AFM phase, where a strong external field creates a high-field slope by changing the magnetization angle between sublattices. However, neither our DFT calculations nor any specific experimental evidence indicates the existence of an AFM phase with a Néel temperature above 400 K.

IV. Discussion and Conclusion

Our analyses indicate that the Mn-V-In sample is essentially Pauli-paramagnetic but contains superparamagnetic clusters that give rise to a magnetic signal in the ZFC/FC and hysteresis measurements. This is in contrast to the theoretical predictions of ferrimagnetism in Mn_2VIn. A likely explanation is off-stoichiometry, which has been firmly established for one phase ($Mn_{2.29}V_{0.6}In$) but, very likely, also occurs in the other two phases. This off-stoichiometry and the unknown crystal structure of the tetragonal phase make it very difficult to identify the metallurgical origin of the magnetic signal.

It is instructive to compare the present superparamagnetism with that investigated by Yuan *et al.* [10], in Heusler-type Ni–Co–Mn–Sb. In both systems, the clear identification of a superparamagnetic signal requires the absence of a ferri- or FM phase, which would otherwise dominate the magnetic signal. On the other hand, the superparamagnetism occurs near the onset of magnetically ordered phases, because completely "nonmagnetic" alloys are trivial in the sense that they are unlikely to contain superparamagnetic regions. A third similarity is that the superparamagnetism is triggered by the chemical composition. However, the actual physical mechanism is different. In the present case, ideal Mn_2VIn is presumably ferrimagnetic, but off-stoichiometry moves the system away from long-range magnetic order. In [10], an FM-AFM transition is triggered by the Co–Ni ratio.

In summary, we have performed a combined theoretical and experimental study of $\mathbf{Mn_2}$VIn. DFT predicts a ferrimagnetic but not half-metallic spin structure in $L2_1$-ordered $\mathbf{Mn_2}$VIn with optimized lattice constants, but lattice compression yields a transition to half-metallicity. Our experiments on arc-melted Mn-V-In show that stoichiometric $\mathbf{Mn_2}$VIn is unstable and the off-stoichiometry destroys the long-range ferrimagnetic order. Nevertheless, the sample exhibits an interesting magnetic behavior, with two maxima in the ZFC magnetization curves. A likely explanation is the existence of two types of superparamagnetic regions. The theoretical calculations indicate the vicinity of a martensitic phase transition, which may play a role in the phase formation, although none of the experimentally involved phases seems to be ferrimagnetic.

Acknowledgment

Z. W. Muthui would like to thank OWSD, IIT Mandi, and DAAD for a Ph.D. scholarship at the University of Nairobi. The work of R. S (interpretation of theoretical and experimental results) was supported by DOE BES under Grant FG02-04ER46152. The authors would like to thank Dr. Kaustav and Mohit of IIT Mandi, for their assistance in sample preparation and magnetic measurements.

REFERENCES

[1] M. A. Tanaka *et al.*, "Preparation of Co_2FeSn Heusler alloy films and magnetoresistance of Fe/MgO/Co_2FeSn magnetic tunnel junctions," *J. Appl. Phys.*, vol. 111, no. 5, p. 053902, Mar. 2012.

[2] I. Galanakis, K. Özdogan, E. Sasioglu, and B. Aktas, "Doping of Mn2VAl and Mn2VSi Heusler alloys as a route to half-metallic antiferromagnetism," *Phys. Rev. B, Condens. Matter*, vol. 75, no. 9, p. 092407, 2007.

[3] A. Ayuela, J. Enkovaara, K. Ullakko, and R. M. Nieminen, "Structural properties of magnetic Heusler alloys," *J. Phys. Condens. Matter*, vol. 11, no. 8, pp. 2017–2026, 1999.

[4] M. Sasaki, P. E. Jönsson, H. Takayama, and H. Mamiya, "Aging and memory effects in superparamagnets and superspin glasses," *Phys. Rev. B, Condens. Matter*, vol. 71, no. 10, p. 104405, Mar. 2005.

[5] W. Zhang *et al.*, "Superparamagnetic behaviour in melt-spun Ni_2FeAl ribbons," *J. Phys. Condens. Matter*, vol. 19, no. 9, p. 096214, 2007.

[6] E. Muñoz-Sandoval, A. D. Chinchure, R. W. A. Hendrikx, and J. A. Mydosh, "Magnetic properties of a new intermetallic compound Ho_2Ni_2Pb," *EPL Europhys. Lett.*, vol. 56, no. 2, p. 302, Oct. 2001.

[7] M. Halder, S. M. Yusuf, A. Kumar, A. K. Nigam, and L. Keller, "Crossover from antiferromagnetic to ferromagnetic ordering in the semi-Heusler alloys $Cu_{1-x}Ni_xMnSb$ with increasing Ni concentration," *Phys. Rev. B, Condens. Matter*, vol. 84, no. 9, p. 094435, Sep. 2011.

[8] M. Kurfiß and R. Anton, "Structural and magnetic properties of vapour deposited thin films of the Heusler alloy Ni_2MnIn," *J. Alloys Compound*, vol. 361, nos. 1–2, pp. 36–39, Oct. 2003.

[9] B. J. Suh, S. H. Baek, and J. Y. Rhee, "Antisite disorder and superparamagnetism in Heusler-like Fe_2VAl : A ^{51}V and ^{27}Al NMR study," *J. Korean Phys. Soc.*, vol. 48, no. 2, pp. 288–292, Feb. 2006.

[10] S. Yuan *et al.*, "Phase separation and superparamagnetism in the martensitic phase of $Ni_{50-x}Co_xMn_{40}Sn_{10}$," *Phys. Rev. B, Condens. Matter*, vol. 93, no. 9, p. 094425, Mar. 2016.

[11] C. Felser and A. Hirohata, Eds., *Heusler Alloys: Properties, Growth, Applications*. Cham, Switzerland: Springer, 2015.

[12] B. Venkateswarlu, P. D. Babu, and N. H. Kumar, "Complex magnetic behavior of the Heusler alloy–$Cu_2Mn_{0.75}Fe_{0.25}Al$," *IEEE Trans. Magn.*, vol. 50, no. 11, Nov. 2014, Art. no. 1002004.

[13] C. S. Lue, Y. Oner, D. G. Naugle, and J. H. Ross, "Magnetism of new semi-Heusler compounds FeVSn and CoVSn," *IEEE Trans. Magn.*, vol. 37, no. 4, pp. 2138–2140, Jul. 2001.

[14] C. S. Lue, J. H. Ross, Jr., K. D. D. Rathnayaka, D. G. Naugle, S. Y. Wu, and W.-H. Li, "Superparamagnetism and magnetic defects in Fe_2VAl and Fe_2VGa," *J. Phys. Condens. Matter*, vol. 13, no. 7, p. 1585, 2001.

[15] V. V. Godlevsky and K. M. Rabe, "Soft tetragonal distortions in ferromagnetic Ni_2MnGa and related materials from first principles," *Phys. Rev. B, Condens. Matter*, vol. 63, no. 13, p. 134407, Mar. 2001.

[16] T. Graf, C. Felser, and S. S. P. Parkin, "Simple rules for the understanding of Heusler compounds," *Prog. Solid State Chem.*, vol. 39, no. 1, pp. 1–50, May 2011.

[17] M. Svedberg, S. Majumdar, H. Huhtinen, P. Paturi, and S. Granroth, "Optimization of $Pr_{0.9}Ca_{0.1}MnO_3$ thin films and observation of coexisting spin-glass and ferromagnetic phases at low temperature," *J. Phys. Condens. Matter*, vol. 23, no. 38, p. 386005, 2011.

[18] C. Zhang, T. Tsuboi, H. Namba, Y. Einaga, and T. Yamamoto, "Enhancement of the coercivity in Co–Ni layered double hydroxides by increasing basal spacing," *Dalton Trans.*, vol. 45, no. 34, pp. 13324–13331, Aug. 2016.

[19] A. K. Nayak, K. G. Suresh, and A. K. Nigam, "Phase coexistence induced by cooling across the first order transition in Ni–Co–Mn–Sb shape memory alloy," *J. Appl. Phys.*, vol. 108, no. 6, p. 063915, 2010.

[20] Y. Chen, Y. Cui, C. Cheng, and Y. Zhao, "Multiple magnetic transitions in SmCoAsO," *AIP Adv.*, vol. 1, no. 4, p. 042134, Nov. 2011.

[21] D. Peddis, C. Cannas, A. Musinu, and G. Piccaluga, "Coexistence of superparmagnetism and spin-glass like magnetic ordering phenomena in a $CoFe_2O_4$-SiO_2 nanocomposite," *J. Phys. Chem. C*, vol. 112, no. 13, pp. 5141–5147, Apr. 2008.

[22] B. Sarkarainadar, "Physical-properties of oxygen-deficient co-based perovskites: $Co(Sr_{1-x}Y_x)O_{3-\delta}$ ($0.05 \leq x \leq 0.4$)," *World J. Condens. Matter Phys.*, vol. 1, no. 4, pp. 145–152, Nov. 2011.

[23] H. Shi and X. He, "Large-scale synthesis and magnetic properties of cubic CoO nanoparticles," *J. Phys. Chem. Solids*, vol. 73, no. 5, pp. 646–650, May 2012.

[24] B. Wang and Y. Liu, "Exchange bias and inverse magnetocaloric effect in Co and Mn co-doped Ni_2MnGa shape memory alloy," *Metals*, vol. 3, no. 1, pp. 69–76, Jan. 2013.